JYX
JYVÄSKYLÄN YLIOPISTO
UNIVERSITY OF JYVÄSKYLÄ

This is a self-archived version of an original article. This version may differ from the original in pagination and typographic details.

Author(s): Chevigny, Romain; Sitsanidis, Efstratios Dimitrios; Schirmer, Johanna; Hulkko, Eero; Myllyperkiö, Pasi; Nissinen, Maija; Pettersson, Mika

Title: Nanoscale Probing of the Supramolecular Assembly in a Two-Component Gel by Near-Field Infrared Spectroscopy

Year: 2023

Version: Published version

Copyright: © 2023 The Authors. Chemistry - A European Journal published by Wiley-VCH GmI

Rights: CC BY 4.0

Rights url: https://creativecommons.org/licenses/by/4.0/

Please cite the original version:

Chevigny, R., Sitsanidis, E. D., Schirmer, J., Hulkko, E., Myllyperkiö, P., Nissinen, M., & Pettersson, M. (2023). Nanoscale Probing of the Supramolecular Assembly in a Two-Component Gel by Near-Field Infrared Spectroscopy. Chemistry : A European Journal, 29(32), Article e202300155. https://doi.org/10.1002/chem.202300155

Chemistry Europe
European Chemical Societies Publishing

WILEY VCH

Excellence in Chemistry Research

Announcing our new flagship journal

- Gold Open Access
- Publishing charges waived
- Preprints welcome
- Edited by active scientists

Meet the Editors of *ChemistryEurope*

Luisa De Cola
Università degli Studi di Milano Statale, Italy

Ive Hermans
University of Wisconsin-Madison, USA

Ken Tanaka
Tokyo Institute of Technology, Japan

Check for updates

Chemistry–A European Journal
Research Article
doi.org/10.1002/chem.202300155
Chemistry Europe
European Chemical Societies Publishing
www.chemeurj.org

Nanoscale Probing of the Supramolecular Assembly in a Two-Component Gel by Near-Field Infrared Spectroscopy

Romain Chevigny,[a] Efstratios D. Sitsanidis,[a] Johanna Schirmer,[a] Eero Hulkko,[a, b] Pasi Myllyperkiö,[a] Maija Nissinen,*[a] and Mika Pettersson*[a]

Abstract: The design of soft biomaterials requires a deep understanding of molecular self-assembly. Here a nanoscale infrared (IR) spectroscopy study of a two-component supramolecular gel is introduced to assess the system's heterogeneity and supramolecular assembly. In contrast to far-field IR spectroscopy, near-field IR spectroscopy revealed differences in the secondary structures of the gelator molecules and non-covalent interactions at three distinct nano-locations of the gel network. A β-sheet arrangement is dominant in single and parallel fibres with a small proportion of an α-helix present, while the molecular assembly derives from strong hydrogen bonding. However, at the crossing point of two fibres, only the β-sheet motif is observed, with an intense π–π stacking contribution. Near-field nanospectroscopy can become a powerful tool for the nanoscale distinction of non-covalent interactions, while it is expected to advance the existing spectroscopic assessments of supramolecular gels.

Introduction

Fourier transform infrared (FTIR) spectroscopy is widely used to probe the secondary structure of proteins and elucidate their conformations and folding.[1–5] Supramolecular gels, especially those consisting of amino acids or small peptides, have gained momentum for the development of soft artificial biomaterials to mimic the extracellular matrix (ECM) for biomedical applications.[6–11] To date, the secondary and higher-order architectures of the gelator molecules are mainly probed by ultraviolet-visible (UV-vis), circular dichroism (CD) and far-field FTIR spectroscopy techniques.[12–19] However, these techniques solely probe the intermolecular interactions of the gelator molecules and higher-order molecular assemblies within the gel network at the macroscale (i.e. in bulk systems). Indeed, the far-field ATR-FTIR spectra of supramolecular gels contain the average of the vibrational bands of the gel system. At the macroscale, the study of the amide I (1600 to 1700 cm^{-1}) and amide II (1500 to 1600 cm^{-1}) regions in peptide-based gels gives valuable information on the secondary structure of the gelator molecules and, consequently, their organization in fibrils and fibres, which form the three-dimensional (3D) gel network.[17–19]

To decipher the molecular/higher-order assemblies and type of interactions in a supramolecular gel system, overcoming the sub-diffraction limit of light and probing at the nanoscale is crucial. Scattering scanning near-field optical microscopy (sSNOM) is an emerging surface spectroscopy technique that has received increasing interest over the past decade.[20] This method combines the topological study of atomic force microscopy (AFM) with the absorptive properties of infrared (IR) radiation on organic molecules. The IR incident radiation is focused at the apex of the probing tip into a highly concentrated electric near-field, which interacts with the sample. The interferometric recording of the scattered light provides infrared spectra at a spatial resolution approximately equivalent to that of the tip (20 nm).[21–28] sSNOM has been used for the analysis of polymeric thin film surfaces,[24,29–35] imaging of cells,[36–40] viruses[41,42] and neurons[43] and the structural elucidation of protein fibrils.[44–46]

Although the secondary structure of protein fibrils has been successfully studied by sSNOM, in supramolecular gels the self-assembly of the gelator molecules (e.g. secondary structure) and the type of non-covalent intermolecular interactions (e.g. hydrogen bonding and π–π stacking) responsible for self-assembly have not yet been studied at the nanoscale. To address the nanoscale probing of molecular self-assembly and elucidate higher-order architectures, such as inter-fibrillar interactions, we introduce sSNOM studies of a two-component amino acid-based organogel, which has been recently introduced by our group (Figure 1).[47] We demonstrate that the high sensitivity of nanoFTIR can distinguish the type of secondary structural features among two structurally similar gelator

[a] R. Chevigny, Dr. E. D. Sitsanidis, J. Schirmer, Dr. E. Hulkko, Dr. P. Myllyperkiö, Prof. M. Nissinen, Prof. M. Pettersson
Department of Chemistry, Nanoscience Center
University of Jyväskylä
P.O. Box Jyväskylä, 35, 40014 JYU (Finland)
E-mail: mika.j.pettersson@jyu.fi
maija.nissinen@jyu.fi

[b] Dr. E. Hulkko
Department of Biological and Environmental Sciences
Nanoscience Center
University of Jyväskylä
P.O. Box Jyväskylä, 35, 40014 JYU (Finland)

Supporting information for this article is available on the WWW under https://doi.org/10.1002/chem.202300155

© 2023 The Authors. Chemistry - A European Journal published by Wiley-VCH GmbH. This is an open access article under the terms of the Creative Commons Attribution License, which permits use, distribution and reproduction in any medium, provided the original work is properly cited.

© 2023 The Authors. Chemistry - A European Journal published by Wiley-VCH GmbH

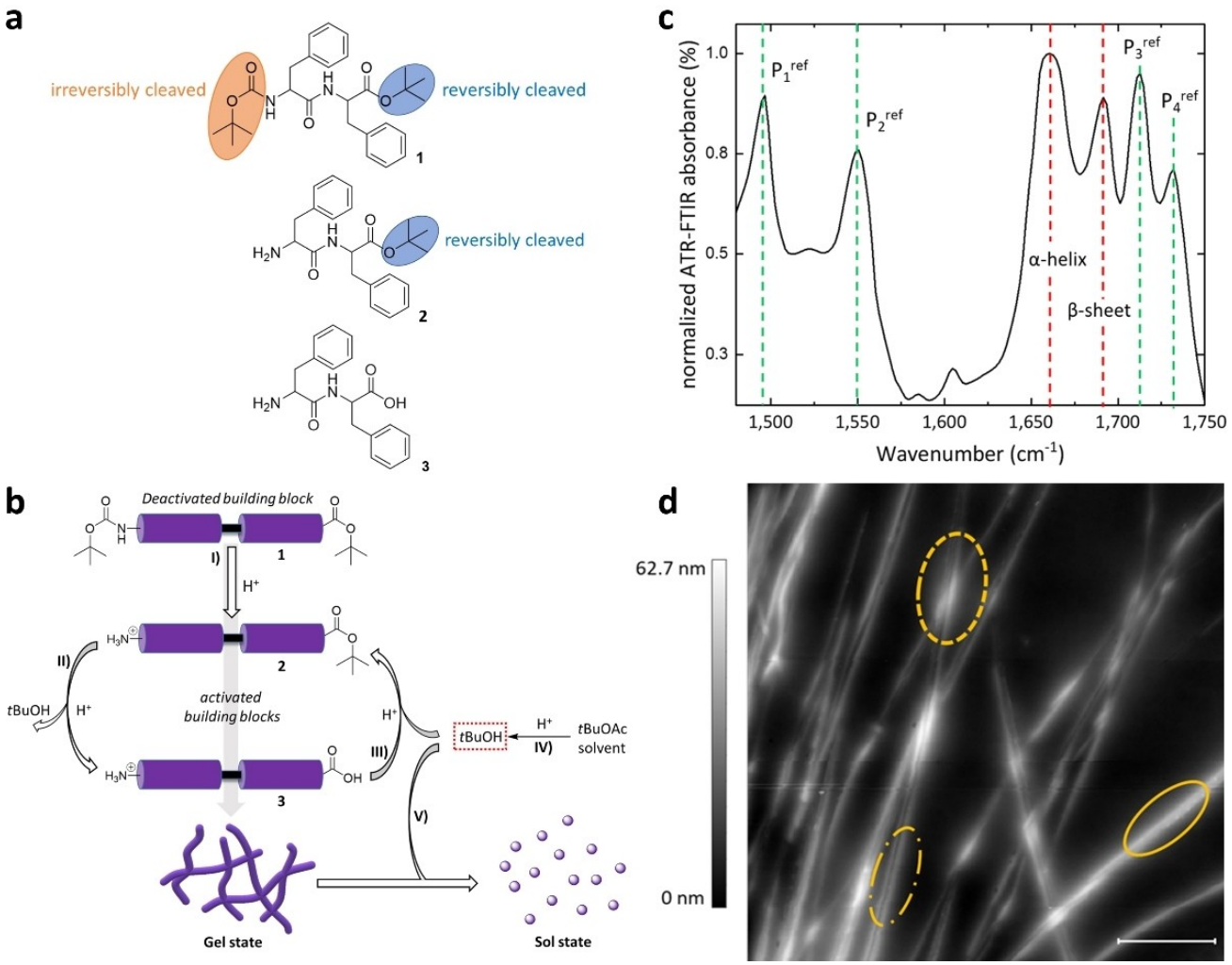

Figure 1. From molecular self-assembly to the macroscopic characteristics of the gel. a) Chemical structures of the protected precursor gelator **1** and activated gelators **2** and **3**. Irreversibly cleaved Boc- group and reversibly cleaved *tert*-butyl groups are highlighted in orange and blue, respectively. b) Schematic depiction of the transient assembly mechanism. *I)* activation of the precursor gelator **1** into the active molecular building blocks **2** and **3**; *II)* hydrolysis of **2**; *III)* esterification of **3**; *IV)* hydrolysis of *t*BuOAc solvent; *V)* dissipation of the gel network. c) ATR-FTIR spectrum of the bulk gel system in the range of 1475 to 1750 cm^{-1} showing the main vibrational bands. Red dashed lines indicate the amide I peaks. The P_1^{ref}, P_2^{ref}, P_3^{ref} and P_4^{ref} peaks (green dashed lines) refer to the vibrations of the functional groups of interest (C=C aromatic stretching, amide II N–H bending, C=O ester stretching and C=O carboxylic acid stretching, respectively). The amide II region shows the N–H bending of the amide group. d) Topography image of the gel's fibres on a gold surface (5×5 μm, scale bar 1 μm). Single fibre (plain circle), crossing point of two single fibres (dashed circle) and two parallel fibres (dash-dotted circle).

molecules. We also introduce sSNOM as a valuable tool for investigating the heterogeneity of multicomponent supramolecular gel networks in high spatial resolution and overcoming surface analysis constraints.

Results and Discussion

Model Gel

In our bimolecular gel system, a chemically active solvent (*tert*-butyl acetate, *t*BuOAc) controls a set of coupled reactions that promote the dynamic assembly event.[47] The two gelator molecules form in situ by the coupled deprotection/protection reactions of the precursor gelator *N-tert*-butoxycarbonyl-L-phenylalanyl-L-phenylalanine-*tert*-butyl ester (Boc-Phe-Phe-O*t*Bu) **1** (Figure 1a). Gelation occurs through the irreversible deprotection of the Boc- group in the presence of the *tert*-butyl group, triggered by the addition of sulphuric acid in the medium, as it forms the activated building block Phe-Phe-O*t*Bu **2** (Figure 1a/b). The *tert*-butyl ester group of **2** is reversibly deprotected to form the free carboxylic acid counterpart Phe-Phe **3**, which reforms to the *tert*-butyl ester **2** through the hydrolysis of the *t*BuOAc solvent. Through hydrolysis, the *t*BuOAc solvent provides the tBu^+ cation needed to esterify **3** towards **2** and generates the secondary solvent *tert*-butyl alcohol (*t*BuOH), which acts antagonistically against the primary solvent *t*BuOAc. Indeed, unlike the free acid **3**, its *tert*-butylated counterpart **2** is soluble in *t*BuOH, thus leading to the progressive dissolution of the supramolecular network.

© 2023 The Authors. Chemistry - A European Journal published by Wiley-VCH GmbH

15213765, 2023, 32, Downloaded from https://chemistry-europe.onlinelibrary.wiley.com/doi/10.1002/chem.202300155 by University Of Jyväskylä Library, Wiley Online Library on [13/07/2023]. See the Terms and Conditions (https://onlinelibrary.wiley.com/terms-and-conditions) on Wiley Online Library for rules of use; OA articles are governed by the applicable Creative Commons License

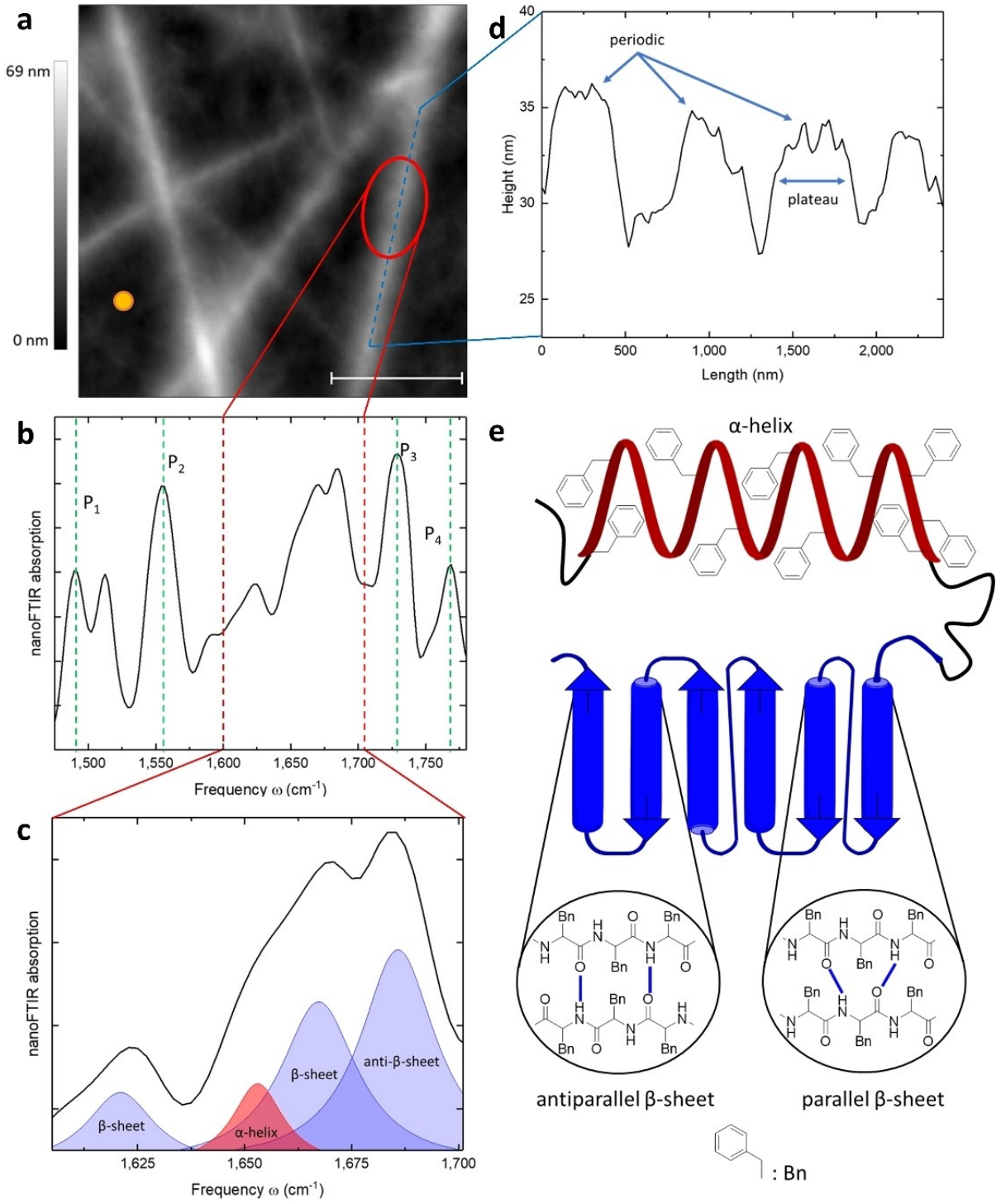

Figure 2. Spectroscopic and structural information of a single fibre. a) Topography image of the formed fibres on a gold surface (3×3 μm, scale bar 1 μm). The orange spot indicates the location of the recorded reference spectrum for b). b) NanoFTIR spectrum of a single fibre recorded at the position marked by the red circle in a). Average of 10 interferograms, 20 ms integration time. A reference spot was taken on the gold surface. P_1, P_2, P_3 and P_4 (green dashed lines) correspond to the vibrational bands of the functional groups of interest (C=C aromatic stretching, N–H amide bending, C=O ester stretching and C=O carboxylic acid stretching, respectively). c) NanoFTIR expansion spectrum of the amide I area (1600–1700 cm^{-1}) indicated by the red dashed lines in b). Experimental spectrum (black curve) and fitting function for each individual peak. Blue fits refer to β-sheet secondary structures and red fit to an α-helix. d) The height profile of the cross-section taken at the position marked by the blue dashed line in a). The obtained features (periodicity and plateau of height) indicate both β-sheet and α-helical structures.[52] e) Schematic representation of the secondary structures adopted by the single fibres.

The hydrolysis/esterification cycles between compounds **2** and **3** control the formation of the supramolecular network. Interestingly, for this dynamic system to initiate the gelation process, both building blocks **2** and **3** are required (Figure S1).

© 2023 The Authors. Chemistry - A European Journal published by Wiley-VCH GmbH

15213765, 2023, 32, Downloaded from https://chemistry-europe.onlinelibrary.wiley.com/doi/10.1002/chem.202300155 by University Of Jyväskylä Library, Wiley Online Library on [13/07/2023]. See the Terms and Conditions (https://onlinelibrary.wiley.com/terms-and-conditions) on Wiley Online Library for rules of use; OA articles are governed by the applicable Creative Commons License

Therefore, the supramolecular network consists of two structurally similar entities differing only at their *C*-terminus (free carboxylic acid and *tert*-butyl ester), which are intimately linked to one another since neither can support gelation individually.

The far-field ATR-FTIR spectrum of the bulk organogel (Figure 1c and Figure S2) shows the characteristic vibrational bands at 1691 cm^{-1} and 1660 cm^{-1}, which correspond to β-sheet and α-helical secondary structures, respectively.[2,4,5] In general, for diphenylalanine-based (Phe-Phe) supramolecular gels, mainly a β-sheet secondary structure (both parallel and anti-parallel) is reported, relating to the strength of π-π stacking and hydrogen bonding interactions.[11,47–51] Therefore, in our study, the obtained peaks P_1 (1496 cm^{-1}, C=C aromatic), P_2 (1550 cm^{-1}, N–H amide II), P_3 (1712 cm^{-1}, *tert*-butyl ester of **2**) and P_4 (1732 cm^{-1}, carboxylic acid of **3**)[2,3] and the amide I region are of primary importance to reveal the heterogeneity in molecular organization and how non-covalent interactions drive the network formation at the nanoscale.

Nanoscale Packing Modes and Interactions in a Single Fibre

The 3D gel network consists of single fibres entangled into wider bundles (Figure 1d).[47,51] Here, we compare the supramolecular interactions, as observed, in a single fibre, along two parallel fibres and at the crossing point of two fibres by near-field spectroscopy, which is an important tool to identify non-covalent interactions responsible for the molecular assembly at the nanoscale. Indeed, in contrast to far-field ATR-FTIR, it enables the selective recording of the nanoscale IR profile of a distinguished higher-order structure, such as a single fibre. Therefore, we recorded the nanoFTIR spectrum at a specific position along an individual fibre (Figure 2a), which showed the four vibrational bands of interest, as already observed in the bulk material (P_1, P_2, P_3 and P_4 marked by the green dashed lines in Figure 2b). It is reasonable to assume that due to intermolecular interactions, the shifts observed for P_3 and P_4 are insufficient to inverse their positions. Therefore, we assign the lower wavenumber peak to P_3 and the higher wavenumber peak to P_4. A summary of the peak positions is presented in Table 1 (Figure S5a and Table S1), along with the reference positions in the spectra of the synthesized gelators (powder materials, Figure S3 and S4) and the bulk gel, measured by far-field ATR-FTIR. Based on the nanoFTIR data, the lower wavenumbers of the P_1 (C=C aromatic), P_3 (C=O ester) and P_4 (C=O carboxylic acid) bands in the single fibre, compared to the synthesized gelators (powder materials), indicate that both functional groups are involved in the assembly event. The results are in accordance with previously reported data for assemblies of the Phe-Phe motif.[11,48–51]

Although the type of interactions is similar at the nanoscale (single fibre/nanoFTIR) and bulk gel (macroscale/ATR-FTIR), their strength is different, as the wavenumbers for both carbonyl group signals are significantly higher in the single fibre spectrum. This suggests that along an individual fibre, the hydrogen bonding originating from the *C*-terminal carbonyl groups of **2** and **3** is weaker compared to the bulk material. This is due to the averaging of the far-field FTIR, which takes all entities and conformations into account. In contrast, at the nanoscale, only the interactions involved in the formation of a single fibre are collected. The downshift of P_4 is much higher than that of P_3, meaning that the carboxylic acid interacts stronger than the ester group. The reason for this is the steric hindrance caused by the bulky *tert*-butyl group and the stronger hydrogen bonding tendency of free carboxylic acids, confirmed by a previously reported study on carboxylic acid complex formation.[52]

A more detailed study of the amide I region (Figure 2c) revealed a convoluted band which gave rise to four distinct peaks upon deconvolution. The minima of the second derivative within the region of interest were used to determine the number of the individual bands for subsequent fitting (see more in Supporting Information). The peak at 1652 cm^{-1} is attributed to an α-helical structure (red fitting curve), while the three peaks at 1627 cm^{-1}, 1669 cm^{-1} and 1690 cm^{-1} correspond to parallel and antiparallel β-sheet structures (blue fitting curves).[4,5] In contrast to previous studies on Phe-Phe-based supramolecular materials where mainly a β-sheet structure is reported,[11,49,50] here the calculated distribution, as obtained by Gaussian fitting (bandwidth, assuming the same intrinsic intensity), is 10% and 90% for α-helical and β-sheet structures, respectively. This highlights the high spatial resolution of nanoFTIR in assessing the structural differences at the nanoscale, compared to the bulk material far-field ATR-FTIR studies at the macroscale.

In addition to spectroscopy recordings, the height profile measurements have also been used to describe the secondary structure of fibres.[53] We obtained the height profile of a cross-section taken at the same spot as the nanoFTIR spectrum (Figure 2d). The presence of a plateau of height indicates an α-helix, whereas periodic features reveal β-sheet structures. There is some difference in observed height between this measurement and the literature[53] but it can be explained by the difference in the structure of the reported gelators. Thus, the height pattern provides information on the secondary structure. Both secondary structures are present in the 3D gel network, while the orientation of the side chains dictates whether the molecular arrangement of the gelators is parallel or antiparallel in the β-sheet motif (Figure 2e).

Nanoscale Packing Modes and Interactions of Two Parallel Fibres in Contact

The molecular arrangement giving rise to a single 1D fibre originates from π-π stacking and hydrogen bonding. For higher-order organizations, however, the strength of the interactions and the type of functional groups involved are affected by the spatial orientation and/or entanglement of the 1D fibres within the supramolecular network. For instance, probing the contact point of two parallel fibres along their longitudinal axes (Figure 3a) reveals differences in the peak intensity and position compared to the IR profile of a single fibre. The 3D topography depiction (Figure 3b) of the two-fibre

© 2023 The Authors. Chemistry - A European Journal published by Wiley-VCH GmbH

15213765, 2023, 32, Downloaded from https://chemistry-europe.onlinelibrary.wiley.com/doi/10.1002/chem.202300155 by University Of Jyväskylä Library, Wiley Online Library on [13/07/2023]. See the Terms and Conditions (https://onlinelibrary.wiley.com/terms-and-conditions) on Wiley Online Library for rules of use; OA articles are governed by the applicable Creative Commons License

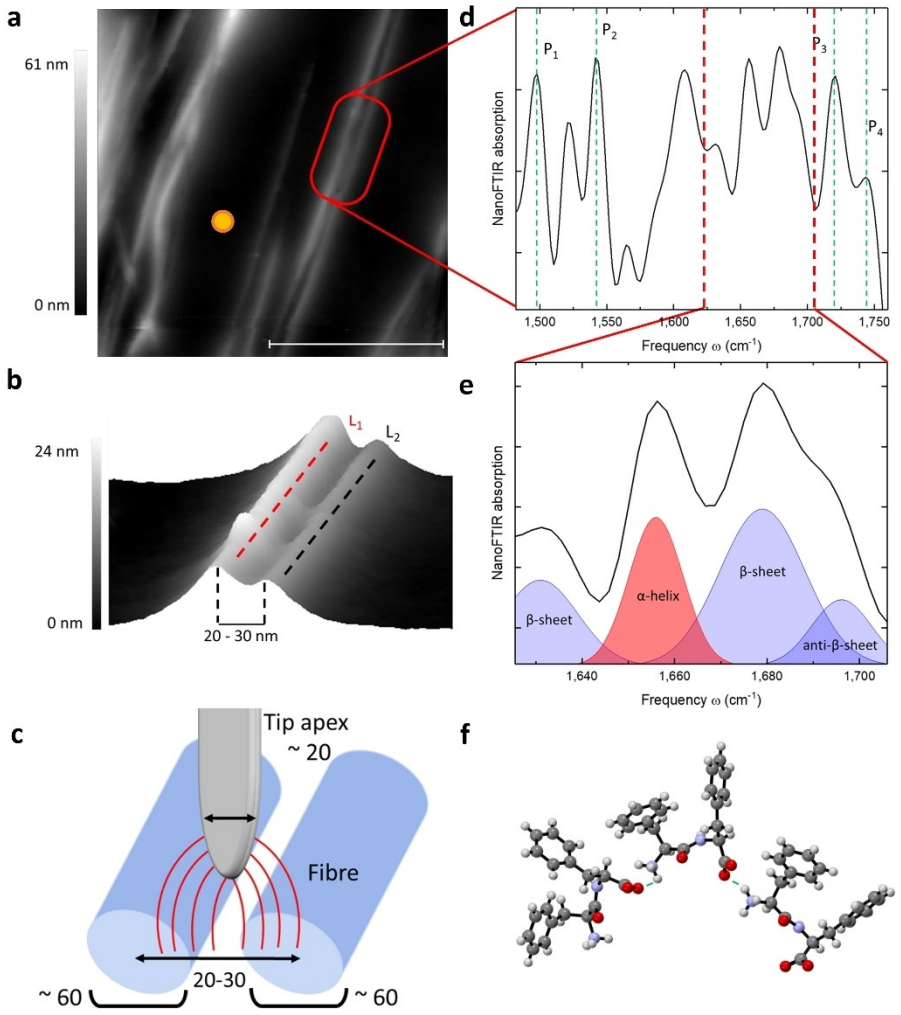

Figure 3. Supramolecular arrangement along two parallel fibres. a) Topography image of two parallel fibres on a gold surface (2×2 μm, scale bar 1 μm). The orange spot indicates the location of the recorded reference spectrum for d). b) 3D magnification of the red rectangle in a), showing two parallel fibres. Vertical dashed lines show the distance between the height maxima. The red (L_1) and black (L_2) dashed lines refer to the cross-section height profile measurement in Figure S6. c) Schematic depiction of the near-field measurement. The probed volume includes the contact point of the two parallel fibres. Numerical values are in nanometres. d) NanoFTIR spectrum of the parallel fibres recorded at the position marked by the red rectangle in a). Average of 10 interferograms, 40 ms integration time. A reference spot was taken on the gold surface. P_1, P_2, P_3 and P_4 (green dashed lines) correspond to the vibrational bands of the functional groups of interest (C=C aromatic stretching, N–H amide bending, C=O ester stretching and C=O carboxylic acid stretching, respectively). e) NanoFTIR spectral expansion of the amide I area (1600–1700 cm^{-1}) indicated by the red dashed lines in d). Experimental spectrum (black curve) and fitting function for each individual peak. Blue fits refer to β-sheet and the red fit to an α-helical structure. f) Schematic depiction of the hydrogen bonding interactions in the molecular arrangement of two adjacent fibres in contact.[55]

system depicts the location of the nanoFTIR measurement. The height of the individual fibres is between 20–30 nm as well as the distance between the height maxima of the cross-section. These values correspond to tubular structures with a diameter of 20–30 nm in contact with each other. The lateral dimension is much larger in the image (~60 nm for each individual fibre) presumably due to the tip convolution effect arising from the AFM probing tip. The recorded image is, therefore, a convolution of the actual object and the finite size tip.[54] As the near-field, generated by the oscillation of the tip on the surface, probes at a spatial resolution of ~20 nm, the recording of the nanoFTIR spectrum covers both fibres and their contact point, allowing us to study the spectral differences compared to a single fibre (Figure 3d). The four bands of interest (P_1, P_2, P_3 and P_4, marked by the green dashed lines) are summarized in Table 1 (see also Figure S5b). The peak corresponding to the aromatic moieties (P_1) is not shifted compared to the ATR-FTIR profile of the gelator molecules **2** and **3** (powder materials). This suggests that the phenyl rings are not involved in stacking interactions along the parallel fibres. However, a small shift of the amide II peak (P_2) is observed, whereas the carbonyl groups P_3 and P_4 show a higher downshift. The results suggest that hydrogen bonding is stronger when two fibres are connected at their longitudinal axes than in a single fibre. As for single fibre, the terminal carbonyl groups (carboxylic acid and ester) show a different shift depending on their steric hindrance and bulkiness.

© 2023 The Authors. Chemistry - A European Journal published by Wiley-VCH GmbH

15213765, 2023, 32, Downloaded from https://chemistry-europe.onlinelibrary.wiley.com/doi/10.1002/chem.202300155 by University Of Jyväskylä Library, Wiley Online Library on [13/07/2023]. See the Terms and Conditions (https://onlinelibrary.wiley.com/terms-and-conditions) on Wiley Online Library for rules of use; OA articles are governed by the applicable Creative Commons License

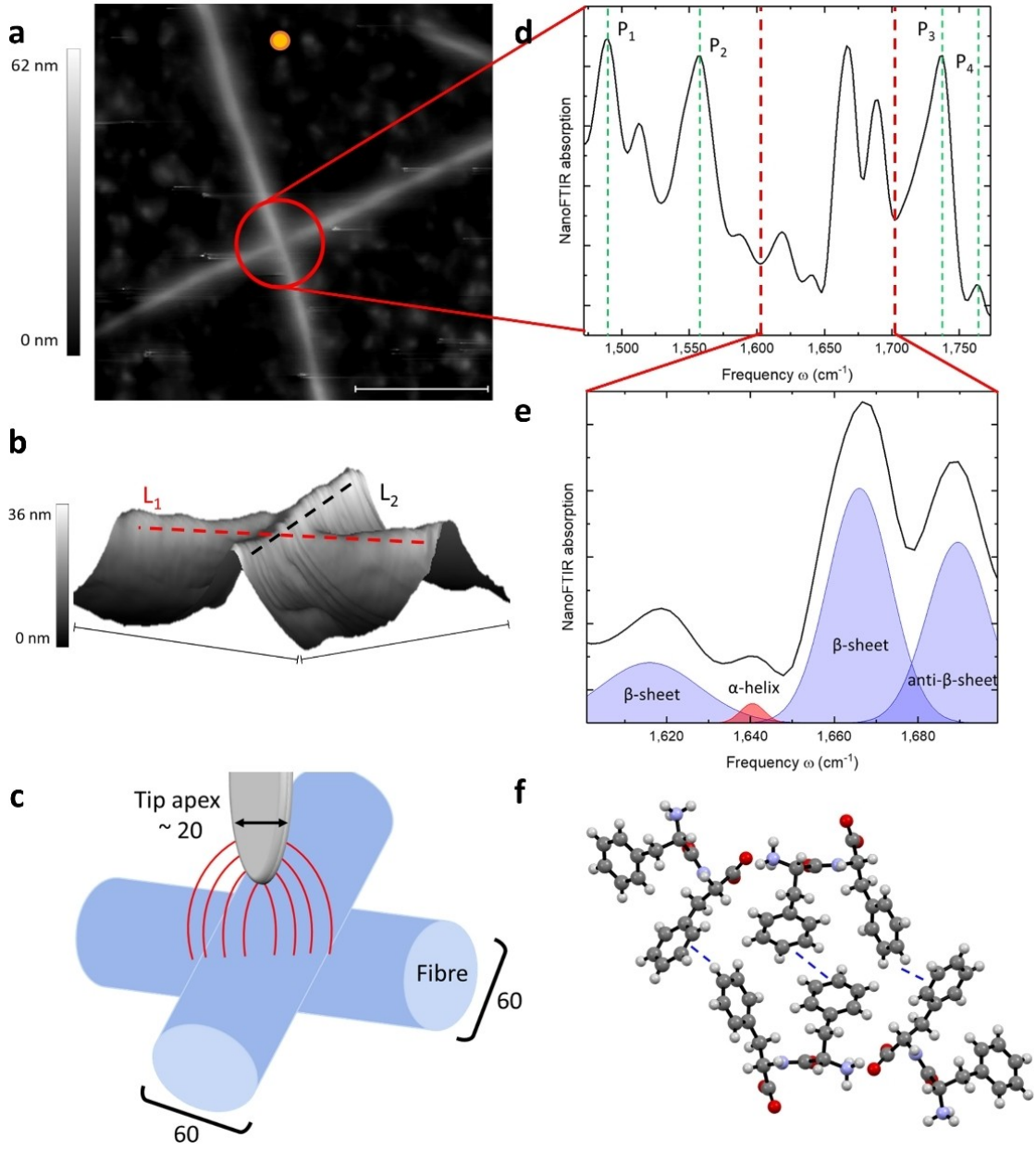

Figure 4. Secondary structure difference at the crossing point of two fibres. a) Topography image of two crossing fibres on a gold surface (3×3 μm, scale bar 1 μm). The orange spot indicates the location of the recorded reference spectrum for d). b) 3D magnification of the red circle in a), showing the crossing point of two fibres (scale bar 800 nm). Dashed lines L_1 (red) and L_2 (black) refer to the cross-section height profile measurement in Figure S7. c) Schematic depiction of the near-field measurement. Numerical values are in nanometres. d) NanoFTIR spectrum of the crossing point of two fibres (obtained from the position marked by the red circle in a). Average of 10 interferograms, 20 ms integration time. A reference spot was taken on a gold surface. P_1, P_2, P_3 and P_4 (green dashed lines) correspond to the vibrational bands of the functional groups of interest (C=C aromatic stretching, N–H amide bending, C=O ester stretching and C=O carboxylic acid stretching, respectively). e) NanoFTIR spectral expansion of the amide I area (1600–1700 cm^{-1}) indicated by the red dashed lines in d). Experimental spectrum (black curve) and fitting function for each individual peak. Blue fits refer to β-sheet and the red fit to an α-helix secondary structure. f) Schematic depiction of the hydrogen bonding and π–π stacking interactions in the molecular arrangement of the two adjacent fibres in perpendicular contact.[55]

The deconvolution of the amide I region reveals four bands (Figure 3e) with equivalent positions to the single fibre IR profile (1653 cm^{-1} corresponding to an α-helical structure (red fitting curve) and the peaks 1626 cm^{-1}, 1679 cm^{-1} and 1691 cm^{-1} corresponding to parallel and antiparallel β-sheet arrangements (blue fitting curves)). The calculated composition by Gaussian fitting (20% and 80% for α-helix and β-sheet, respectively) is also qualitatively similar to the single fibre nanoFTIR measurements. Therefore, although the strength of the supramolecular interactions differs with the spatial location of the fibres, the secondary structures are not affected.

A cross-section of each fibre (L_1 (red) and L_2 (black) lines, Figure 3b) was also used to assess the secondary structure. The corresponding height profile (Figure S6) shows the character-

© 2023 The Authors. Chemistry - A European Journal published by Wiley-VCH GmbH

15213765, 2023, 32, Downloaded from https://chemistry-europe.onlinelibrary.wiley.com/doi/10.1002/chem.202300155 by University Of Jyväskylä Library, Wiley Online Library on [13/07/2023]. See the Terms and Conditions (https://onlinelibrary.wiley.com/terms-and-conditions) on Wiley Online Library for rules of use; OA articles are governed by the applicable Creative Commons License

Table 1. P_1, P_2, P_3 and P_4 peak positions (cm^{-1}) in the nanoFTIR spectrum of crossed, parallel, and single fibres, their reference position in the ATR-FTIR spectra of the bulk gel and the synthesized gelators **2** and **3**.

	Crossing fibres	Single fibre	Parallel fibre	Gelator **2**	Gelator **3**	Bulk gel
P_1 C=C stretch. aromatic	**1489**	1488	1496	1496	1497	1493
P_2 N–H bend.	**1556**	1557	1546	/	1550	1550
P_3 C=O stretch. ester	**1729**	1727	1720	1732	/	1712
P_4 C=O stretch. carbox. acid	**1761**	1754	1743	/	1780	1731

istic plateau of an α-helix, although wider, while no characteristic features of a β-sheet arrangement were observed for the L_1 fibre. On the contrary, L_2 fibre shows a relatively constant height profile. Thus, the proximity of the two fibres seems to hinder the topographical determination of the secondary structure. However, the information could be obtained from the spectroscopic profile. A depiction of the potential interactions responsible for the gelator's assembly mode in this spatial location is given in Figure 3f. A previously reported crystal structure of the dipeptide Phe-Phe[55] clearly shows hydrogen bonding between the carboxylic acid and the amine groups. In addition, interactions involving the amide group are observed.

Structural Differences at the Crossing Point of Two Single Fibres

In addition to the two parallel fibres, we aimed to decipher the supramolecular interactions at the crossing point of two fibres (Figure 4a). The height of each fibre is approximately 20 nm, while the 3D magnification shows that the fibres fuse at the crossing point. Therefore, the near-field resolution (~20 nm) can probe the fibre interactions (Figures 4b and 4c). The nanoFTIR spectrum at this particular point reveals an opposite trend to the parallel fibres (Figure 4d). Indeed, the peak of the aromatic moieties (P_1) of the building blocks are shifted (Table 1 and Figure S5c), showing their involvement in molecular packing. Interestingly, the peak of the bulky *tert*-butyl group (P_3) is not shifted, in contrast to the free carboxylic acid (P_4). However, the shift is lower compared to the single and parallel fibres. The results indicate that when two fibres interact perpendicularly (crossing point), the phenyl rings of the molecules interact to maintain their secondary structure and are supported by the hydrogen bonding originating from the carboxylic acid groups (Figure 4f).

The deconvolution of the amide I region of the spectrum reveals a deviating trend from the previous spatial locations (Figure 4e). The presence of the four bands attributed to α-helix (red fitting curve, 1651 cm^{-1}), parallel β-sheet (blue fitting curves, 1627 cm^{-1} and 1670 cm^{-1}) and antiparallel β-sheet (blue fitting curves 1790 cm^{-1}) is also observed at the crossing point, and their band positions are quantitatively similar. However, the calculated relative composition of the secondary structure differs. Indeed, Gaussian fitting yielded 96% of β-sheet structures and 4% of α-helical structures. In contrast to the single and two parallel fibres, the secondary structure at the crossing point of two fibres is altered and is now dominated by a β-sheet arrangement (Table 2).

Table 2. Peak positions (cm^{-1}) and composition (%) of the secondary structure at three different spatial locations of the gel network.

	Single fibre		Parallel fibres		Crossing fibres	
β-sheet	1626		1626		1627	
β-sheet	1669	**90%**	1679	**80%**	1670	**96%**
anti-β-sheet	1690		1691		1690	
α-helix	1652	**10%**	1653	**20%**	1651	**4%**

The cross-sections of the two perpendicular fibres and the corresponding height profile (L_1 (red) and L_2 (black) Figure 4b and Figure S7) show a plateau of height for the L_1 fibre (characteristic of the α-helix structure), although shorter than for the single fibre. The height profiles do not give detailed structural information at the crossing point. Similarly to the parallel fibres, this is observed when the two fibres are adjacent. However, the structural information is evident on the spectroscopic profile. The height profile of the L_1 fibre clearly indicates the contact point, at which it interacts with the L_2 fibre. Figure 4f depicts the interactions maintaining the structure at the crossing point. The interpretation is supported by the previously reported Phe-Phe crystal structure,[55] which shows both π–π and CH-π stacking of the phenyl rings.

It is of note that drying conditions alter the fibrous network depending on the process,[56] and hence the vibrational frequencies of the freeze-dried (sSNOM) and room temperature dried (bulk gel) materials may differ. Freeze drying allows to study the closest state to the 3D material network whereas drying at room temperature distorts the fibre arrangement (restructuration over the slow collapse of the material induced by solvent evaporation). The frequencies for P_3 and P_4 in the bulk gel state are lower than those at the nanoscale, presumably due to the difference in drying conditions (see Table 1). Additionally, the sSNOM spectra were taken only at a few specific locations and a much larger data set would be needed for statistically meaningful comparison of frequencies.

Conclusion

Our study aimed to decipher the non-covalent interactions and the corresponding secondary structure of the gel fibres at a nanoscale spatial resolution with infrared spectroscopy. Depending on the spatial location of the fibrous gel network, the spectral differences provide additional insight into the driving forces leading to its formation.

Our observations demonstrate that the formation of a single fibre and the parallel orientation of two single fibres is dictated

© 2023 The Authors. Chemistry - A European Journal published by Wiley-VCH GmbH

15213765, 2023, 32, Downloaded from https://chemistry-europe.onlinelibrary.wiley.com/doi/10.1002/chem.202300155 by University Of Jyväskylä Library, Wiley Online Library on [13/07/2023]. See the Terms and Conditions (https://onlinelibrary.wiley.com/terms-and-conditions) on Wiley Online Library for rules of use; OA articles are governed by the applicable Creative Commons License

mainly by hydrogen bonding, mainly originating from the carboxylic acid group, since its shift is higher than that of the bulky ester group. In both configurations, the secondary structure is constant, with a significant contribution of β-sheet and a small proportion of α-helix. However, there is a tremendous change at the crossing point of two fibres, where a preference towards π-π stacking with a weaker contribution of hydrogen bonding is observed. The secondary structure is dominated by β-sheet with a negligible proportion of α-helix. Our findings are consistent with the previously reported results on similar supramolecular gels studied as bulk materials by far-field IR and other spectroscopic methods.[11,48,49,51] However, nanoFTIR spectroscopy gives a deeper insight into the heterogeneity of supramolecular systems and increases our understanding of the molecular assembly modes in relation to the features of the supramolecular network at the nanoscale.

The sSNOM, therefore, proved to be a sensitive and reliable technique to study soft supramolecular materials, as it enables the direct spectroscopic assessment of the molecular building block arrangement while overcoming surface analysis constraints.[57] Thus, this technique has the potential to become a routine spectroscopic assessment tool and expand the range of techniques to study soft supramolecular gels.

Authors contributions

R.C.: Conceptualization, Investigation, Formal Analysis, Validation, Writing - original draft, review & editing. **E.D.S.**: Conceptualization, Investigation, Writing - review & editing. **J.S.**: Investigation, Writing - review & editing. **E.H.**: Investigation, Resources, Writing - review & editing. **P.M.**: Investigation, Resources. **M.N.**: Supervision. **M.P.**: Supervision, Funding acquisition.

Acknowledgements

The authors would like to acknowledge the Jane and Aatos Erkko foundation for supporting the current work.

Conflict of Interest

The authors declare no conflict of interest.

Data Availability Statement

The data that support the findings of this study are available from the corresponding author upon reasonable request.

Keywords: IR spectroscopy · near-field · secondary structure · self-assembly · transient gel

[1] S. Cai, B. R. Singh, *Biophys. Chem.* **1999**, *80*, 7–20.
[2] A. Barth, *Prog. Biophys. Mol. Biol.* **2000**, *74*, 141–173.
[3] A. Barth, C. Zscherp, *Q. Rev. Biophys.* **2002**, *35*, 369–430.
[4] A. Barth, *Biochim. Biophys. Acta Bioenerg.* **2007**, *1767*, 1073–1101.
[5] J. Kong, S. Yu, *Acta Biochim. Biophys. Sin.* **2007**, *39*, 549–559.
[6] J. D. Tang, C. Mura, K. J. Lampe, *J. Am. Chem. Soc.* **2019**, *141*, 4886–4899.
[7] W. K. Restu, Y. Nishida, S. Yamamoto, J. Ishii, T. Maruyama, *Langmuir* **2018**, *34*, 8065–8074.
[8] J. Fraczyk, W. Lipinski, A. Chaberska, J. Wasko, K. Rozniakowski, Z. J. Kaminski, M. Bogun, Z. Draczynski, E. Menaszek, E. Stodolak-Zych, M. Kaminska, B. Kolesinska, *Molecules* **2018**, *23*, 1–19.
[9] E. González-Díaz, S. Varghese, *Gels* **2016**, *2*, 20.
[10] G. Fichman, E. Gazit, *Acta Biomater.* **2014**, *10*, 1671–1682.
[11] X. Yan, P. Zhu, J. Li, *Chem. Soc. Rev.* **2010**, *39*, 1877–1890.
[12] L. J. White, C. Wark, L. Croucher, E. R. Draper, J. R. Hiscock, *Chem. Commun.* **2020**, *56*, 9557–9560.
[13] E. D. Sitsanidis, C. C. Piras, B. D. Alexander, G. Siligardi, T. Jávorfi, A. J. Hall, A. A. Edwards, *Chirality* **2018**, *30*, 708–718.
[14] Z. Shen, Y. Jiang, T. Wang, M. Liu, *J. Am. Chem. Soc.* **2015**, *137*, 16109–16115.
[15] J. T. van Herpt, M. C. A. Stuart, W. R. Browne, B. L. Feringa, *Chem. Eur. J.* **2014**, *20*, 3077–3083.
[16] J. Shi, Y. Gao, Z. Yang, B. Xu, *Beilstein J. Org. Chem.* **2011**, *7*, 167–172.
[17] E. Parisi, A. M. Garcia, D. Marson, P. Posocco, S. Marchesan, *Gels* **2019**, *5*, 5.
[18] L. Chen, K. Morris, A. Laybourn, D. Elias, M. R. Hicks, A. Rodger, L. Serpell, D. J. Adams, *Langmuir* **2010**, *26*, 5232–5242.
[19] E. R. Draper, D. J. Adams, *Chem. Soc. Rev.* **2018**, *47*, 3395–3405.
[20] X. Chen, D. Hu, R. Mescall, G. You, D. N. Basov, Q. Dai, M. Liu, *Adv. Mater.* **2019**, *31*, 1804774.
[21] S. Mastel, A. A. Govyadinov, T. V. A. G. De Oliveira, I. Amenabar, R. Hillenbrand, *Appl. Phys. Lett.* **2015**, *106*, 1–6.
[22] F. Huth, A. Govyadinov, S. Amarie, W. Nuansing, F. Keilmann, R. Hillenbrand, *Nano Lett.* **2012**, *12*, 3973–3978.
[23] L. Mester, A. A. Govyadinov, R. Hillenbrand, *Nat. Photonics* **2022**, *11*, 377–390.
[24] J. Kim, W. Lee, H. Kim, D. Y. Ryu, H. Ahn, B. Chae, *Spectrochim. Acta A. Mol. Biomol. Spectrosc.* **2022**, *274*, 121095.
[25] I. Amenabar, S. Poly, M. Goikoetxea, W. Nuansing, P. Lasch, R. Hillenbrand, *Nat. Commun.* **2017**, *8*.
[26] C. Westermeier, A. Cernescu, S. Amarie, C. Liewald, F. Keilmann, B. Nickel, *Nat. Commun.* **2014**, *5*, 1–6.
[27] R. Krutokhvostov, A. A. Govyadinov, J. M. Stiegler, F. Huth, A. Chuvilin, P. S. Carney, R. Hillenbrand, *Opt. Express* **2012**, *20*, 593.
[28] T. Taubner, R. Hillenbrand, F. Keilmann, *Appl. Phys. Lett.* **2004**, *85*, 5064–5066.
[29] T. E. Tesema, R. Mcfarland-Porter, E. Zerai, J. Grey, T. G. Habteyes, *J. Phys. Chem. C* **2022**, *126*, 7764–7772.
[30] N. Mrkyvkova, A. Cernescu, Z. Futera, A. Nebojsa, A. Dubroka, M. Sojkova, M. Hulman, E. Majkova, M. Jergel, P. Siffalovic, F. Schreiber, *J. Phys. Chem. C* **2021**, *125*, 9229–9235.
[31] A. M. Siddiquee, A. Houri, K. A. Messalea, J. Lin, T. Daeneke, B. Abbey, A. Mechler, S. Kou, *J. Phys. Chem. Lett.* **2020**, *11*, 9476–9484.
[32] S. Berweger, D. M. Nguyen, E. A. Muller, H. A. Bechtel, T. T. Perkins, M. B. Raschke, *J. Am. Chem. Soc.* **2013**, *135*, 18292–18295.
[33] M. Meyns, S. Primpke, G. Gerdts, *Anal. Methods* **2019**, *11*, 5195–5202.
[34] L. Mester, A. A. Govyadinov, S. Chen, M. Goikoetxea, R. Hillenbrand, *Nat. Commun.* **2020**, *11*, 1–10.
[35] M. Goikoetxea, I. Amenabar, S. Chimenti, M. Paulis, J. R. Leiza, R. Hillenbrand, *Macromolecules* **2021**, *54*, 995–1005.
[36] S. Bhagia, J. Ďurkovič, R. Lagaňa, M. Kardošová, F. Kačík, A. Cernescu, P. Schäfer, C. G. Yoo, A. J. Ragauskas, *ACS Sustainable Chem. Eng.* **2022**, *10*, 3016–3026.
[37] V. M. R. Zancajo, T. Lindtner, M. Eisele, A. J. Huber, R. Elbaum, J. Kneipp, *Anal. Chem.* **2020**, *92*, 13694–13701.
[38] K. Kanevche, D. J. Burr, D. J. Nürnberg, P. K. Hass, A. Elsaesser, J. Heberle, *Commun. Biol.* **2021**, *4*, 1–8.
[39] K. J. Kaltenecker, T. Gölz, E. Bau, F. Keilmann, *Sci. Rep.* **2021**, *11*, 1–12.
[40] H. Amrania, L. Drummond, R. C. Coombes, S. Shousha, L. Woodley-Barker, K. Weir, W. Hart, I. Carter, C. C. Phillips, *Faraday Discuss.* **2016**, *187*, 539–553.
[41] S. Gamage, M. Howard, H. Makita, B. Cross, G. Hastings, M. Luo, Y. Abate, *PLoS One* **2018**, *13*, 1–12.
[42] M. Brehm, T. Taubner, R. Hillenbrand, F. Keilmann, *Nano Lett.* **2006**, *6*, 1307–1310.

© 2023 The Authors. Chemistry - A European Journal published by Wiley-VCH GmbH

15213765, 2023, 32, Downloaded from https://chemistry-europe.onlinelibrary.wiley.com/doi/10.1002/chem.202300155 by University Of Jyväskylä Library, Wiley Online Library on [13/07/2023]. See the Terms and Conditions (https://onlinelibrary.wiley.com/terms-and-conditions) on Wiley Online Library for rules of use; OA articles are governed by the applicable Creative Commons License

[43] R. O. Freitas, A. Cernescu, A. Engdahl, A. Paulus, J. E. Levandoski, I. Martinsson, E. Hebisch, C. Sandt, G. K. Gouras, C. N. Prinz, T. Deierborg, F. Borondics, O. Klementieva, *Cells* **2021**, *10*, 1–15.
[44] I. Amenabar, S. Poly, W. Nuansing, E. H. Hubrich, A. A. Govyadinov, F. Huth, R. Krutokhvostov, L. Zhang, M. Knez, J. Heberle, A. M. Bittner, R. Hillenbrand, *Nat. Commun.* **2013**, *4*, 10.1038/ncomms3890.
[45] M. Paulite, Z. Fakhraai, I. T. S. Li, N. Gunari, A. E. Tanur, G. C. Walker, *J. Am. Chem. Soc.* **2011**, *133*, 7376–7383.
[46] M. Dendisová, A. Jeništová, A. Parchaňská-Kokaislová, P. Matějka, V. Prokopec, M. Švecová, *Anal. Chim. Acta* **2018**, *1031*, 1–14.
[47] R. Chevigny, J. Schirmer, C. C. Piras, A. Johansson, E. Kalenius, D. K. Smith, M. Pettersson, E. D. Sitsanidis, M. Nissinen, *Chem. Commun.* **2021**, *57*, 10375–10378.
[48] R. Huang, R. Su, W. Qi, J. Zhao, Z. He, *Nanotechnology* **2011**, *22*, 245609.
[49] X. Yan, Y. Cui, Q. He, K. Wang, J. Li, *Chem. Mater.* **2008**, *20*, 1522–1526.
[50] M. Reches, E. Gazit, *Isr. J. Chem.* **2005**, *45*, 363–371.
[51] S. Marchesan, A. v. Vargiu, K. E. Styan, *Molecules* **2015**, *20*, 19775–19788.
[52] K. B. Beć, Y. Futami, M. J. Wójcik, T. Nakajima, Y. Ozaki, *J. Phys. Chem. A* **2016**, *120*, 6170–6183.
[53] R. Xing, C. Yuan, S. Li, J. Song, J. Li, X. Yan, *Angew. Chem. Int. Ed.* **2018**, *57*, 1537–1542; *Angew. Chem.* **2018**, *130*, 1553–1558.
[54] J. Canet-Ferrer, E. Coronado, A. Forment-Aliaga, E. Pinilla-Cienfuegos, *Nanotechnology* **2014**, *25*, 395703.
[55] C. H. Görbitz, *Chem. Eur. J.* **2001**, *7*, 5153–5159.
[56] L. L. E. Mears, E. R. Draper, A. M. Castilla, H. Su, Z. B. Dietrich, M. C. Nolan, G. N. Smith, J. Doutch, S. Rogers, R. Akhtar, H. Cui, D. J. Adams, *Biomacromolecules* **2017**, *18*, 3531–3540.
[57] J. Schirmer, R. Chevigny, A. Emelianov, E. Hulkko, A. Johansson, P. Myllyperkiö, E. D. Sitsanidis, M. Nissinen, M. Pettersson *Phys. Chem. Chem. Phys.* **2023**, *25*, 8725–8733.

Manuscript received: January 17, 2023
Accepted manuscript online: March 15, 2023
Version of record online: April 27, 2023

© 2023 The Authors. Chemistry - A European Journal published by Wiley-VCH GmbH

15213765, 2023, 32, Downloaded from https://chemistry-europe.onlinelibrary.wiley.com/doi/10.1002/chem.202300155 by University Of Jyväskylä Library, Wiley Online Library on [13/07/2023]. See the Terms and Conditions (https://onlinelibrary.wiley.com/terms-and-conditions) on Wiley Online Library for rules of use; OA articles are governed by the applicable Creative Commons License